Distinct microbial response to organic matter from nitrogen-starved and virus-infected phytoplankton

Shira Givati (1, 2), Eyal Rahav (2, 3, 4), Osnat Weissberg (1), Dikla Aharonovich (1), Noga Barak (1), Qinglu Zeng (5) and Daniel Sher (1)

(1) Department of Marine Biology, University of Haifa, Haifa, Israel

(2) Israel Oceanographic and Limnological Research, National Institute of Oceanography, Tel Shikmona, P.O. Box 8030, Haifa 31080, Israel

(3) Institute of Marine Science, University of California, Santa Cruz, CA, USA.

(4) Department of Earth and Environmental Science, Ben-Gurion University of the Negev, Beer Sheva, Israel.

(5) Department of Ocean Science, Hong Kong University of Science and Technology. Hong Kong SAR, China.

Abstract

When phytoplankton die they release dissolved organic matter (DOM) that feeds co-occurring heterotrophic bacteria. We show that death due to phage infection and nitrogen starvation result in different changes to the macromolecular structure of *Prochlorococcus*, a globally abundant cyanobacterium, and that the resulting DOM elicits different microbial responses. Viral infection led to increased RNA and DNA content in *Prochlorococcus* whereas nitrogen starvation led to a lower protein content. DOM released from phage-infected cells induced high secondary (bacterial) production, while DOM from starved cells increased dark (heterotrophic) primary production in natural microbial communities from the oligotrophic Eastern Mediterranean Sea. Through 16S and 18S amplicon sequencing, metagenomics, and laboratory experiments we identify

Alteromonadaceae and *Rhodobacteraceae* as heterotrophic taxa responding differently to the two DOM sources. We propose that distinct forms of phytoplankton mortality drive shifts in microbial community metabolism, including differential activity of pathways for heterotrophic carbon fixation, likely through anaplerotic reactions.

Introduction

Heterotrophic bacteria in the ocean rely on dissolved organic matter (DOM) released by phytoplankton, including cyanobacteria, as a primary resource for growth (*1*, *2*). DOM is released by phytoplankton as they grow (e.g. through exudation or vesicle release, (*3*)), and as they die, with the specific cause of death potentially affecting the biochemical structure of the phytoplankton and the composition of the released DOM. For example, *Prochlorococcus*, which is the numerically most abundant phytoplankton cell in the oligotrophic oceans (*4*), contributes ~8.5% of the net global marine primary productivity estimated at ~4 Gt C y^{-1} (*5*). As *Prochlorococcus* cells die, they release a diverse mixture of organic compounds, thereby altering the complex DOM pool in the water column (*6–8*). *Prochlorococcus* die mostly through grazing, phage infection and "other" sources of mortality such as UV damage and, potentially, nutrient starvation, but the relative contribution of each cause of death is currently not well constrained. Estimates range between ~66-96% for grazing, 4-40% for phage infection and 1-27% for "other" sources of mortality including starvation (*9–12*). Given that the pulse of organic carbon (C) released when *Prochlorococcus* cells die could account for more than 75% of the daily production at the surface of the oligotrophic ocean (*13*), understanding what affects the composition of this

photosynthetically fixed C and how it affects the surrounding microbial ecosystem could be of significant biogeochemical and ecological importance.

Different types of mortality, such as starvation and phage infection, can alter the composition of released DOM because each cause of death is associated with distinct changes in cellular physiology, resource allocation and macromolecular structure. *Prochlorococcus* cells experiencing nitrogen starvation in the lab have decreased levels of protein and RNA along with elevated carbon content, potentially from storage carbohydrates or lipids (*14*, *15*). Similar changes are seen also in other phytoplankton (*16*, *17*). In contrast, little is known about how virus or phage infection affects the macromolecular structure of phytoplankton, but since phage infections results in the production of protein- and nucleic-acid rich virions, these pools are expected to increase (*18*). Indeed, phage infection has been shown to change host metabolism and biochemical composition (metabolite composition, (*19–21*)). As the cells die and lyse, the changes in macromolecular structure are expected to result in concomitant changes in the released DOM (*22*, *23*).

Once DOM is released from the dying cells, it fuels secondary bacterial production and growth by surrounding heterotrophic bacteria (*24*). During exponential growth in the lab, *Prochlorococcus* releases a variety of organic compounds, including highly labile compounds - amino acids and carboxylic acids such as pyruvate, acetate, and formate (*6*, *25–29*). As the cells die and lyse, they release also cell biomass, which is expected to be enriched in larger and more complex macromolecules such as RNA, DNA, large protein complexes, lipids and other storage polymers. *Prochlorococcus* viral lysate was found to contain more labile, bioavailable DOM (e.g., amino acids, protein-like, and low-molecular-weight compounds), promoting greater bacterial growth than *Prochlorococcus* exudate (*22*). In addition, each of these different types of macromolecules

can fuel the growth of different heterotrophic bacteria (*30–33*). Therefore, it is expected that changes in the biochemical structure of the cells due to different forms of mortality could impact the structure and function of surrounding heterotrophic communities. Indeed, previous studies have suggested that phytoplankton cell lysis due to viral infection (including in *Prochlorococcus*) enhances net productivity and organic matter recycling, significantly more than in ecosystems with low viral infection (*22*, *34–37*). In the ocean, this process is known as the "viral shunt" (*38*, *39*), which plays a crucial role in oceanic biogeochemical cycles by influencing the microbial loop and facilitating the recycling of organic carbon within the marine environment (*34*).

Here, we directly compare how nitrogen starvation and phage infection affect cell quotas of protein, RNA and DNA in *Prochlorococcus* (Figure 1A). We chose to measure these major macromolecular pools as they are the main constituents of cell biomass, determining the elemental ratio of the cells (*40*, *41*). These macromolecules are also emerging as important variables in phytoplankton models from the cellular to ocean scales (*15*, *42*). We then amended surface seawater from the oligotrophic Eastern Mediterranean Sea (EMS) with DOM derived either from nitrogen-starved *Prochlorococcus* (hereafter referred to as treatment nSM) or viral lysate (treatment vSM) (Figure 1A). As expected, we observed increased secondary production due to vSM, but surprisingly we also observed increased dark carbon fixation (DCF) in response to nSM. To investigate the microbial taxa driving this response (i.e., fix CO_2 in response to nSM), we employed 16S and 18S amplicon sequencing, metagenomic analyses and targeted experiments using specific bacterial isolates. Ultimately, by dissecting the differential release of organic compounds under starvation and phage infection, we aim to gain a deeper understanding of *Prochlorococcus*'s role in marine carbon cycling and its complex interactions within ambient marine microbial ecosystem.

Results and discussion

Phage infection and nitrogen starvation differently affect Prochlorococcus macromolecular composition

We first compared how phage infection and nitrogen starvation influence the macromolecular composition of *Prochlorococcus* MED4 (Figure 1). Cultures were infected by myovirus P-HM2 during early to mid-logarithmic growth, with samples collected after 12 hours post infection (hpi, after one round of infection and lysis (*19*)), and after 36 hpi when most of the culture has been lysed (likely after several rounds of infections) (Figure 1B). The uninfected cultures were sampled at the same time points, as well as during mid-decline, following the onset of nitrogen starvation (day 14, Figure S1C (*43*)). Protein quotas per cell, and to lesser extent those of RNA and DNA, decreased in the N-starved *Prochlorococcus* (Figure 1C-E), consistent with prior observations (*14*, *15*). In contrast, RNA and DNA quotas increased for the infected *Prochlorococcus,* and protein quotas remained unchanged (Figure 1C-E).

The increase in intracellular DNA is consistent with synthesis of phage genomic DNA, since P-HM2 has a double-stranded DNA genome (*44*), but the increase in cellular RNA is more perplexing. In most cells, ribosomes contain ~80-90% of the total RNA (*45*), and if this is true in this case it would suggest that the number of ribosomes remains similar or even increases, despite phage infection shutting down major aspects of cell physiology (*46*). A previous study of P-HM2 infection in *Prochlorococcus* MED4 showed a decline in host transcripts related to translation and ribosomal proteins, with phage-derived mRNA levels exceed those of the host genes (*47*). Some phages encode ribosomal proteins such as bS21 and bL12, which could potentially help stabilize the host ribosomes and/or increase their production (*48*, *49*), but no such proteins have been

described in P-HM2. It is possible that P-HM2 encodes other proteins or RNAs that stabilize the ribosome. Alternatively, it is possible that most of the measured RNA is in fact phage RNA, and in this case it is possible that ribosomes are in fact depleted, as observed in SAR11, where a substantial fraction (7–15%) of infected cells were found to be 'ribosome-deprived zombie cells' (*50*). Even if this is true, phage P-HM2 is still able to tightly control the metabolism of its hosts, including potentially protein translation rates, thus avoiding mispackaging of new virions with host rather than viral DNA (*47*, *51*).

The DOM released following cell lysis due to phage infection ("viral spent media", vSM) and nitrogen starvation ("nitrogen-starved spent media", nSM) also differed. Dissolved organic carbon (DOC) was approximately 2 to 3 times higher in the spent media from nitrogen-starved *Prochlorococcus* (nSM) compared to that from infected *Prochlorococcus* (vSM) (500–650 µmol C L^{-1} versus 200–250 µmol C L^{-1}, respectively, Figure 1G). In contrast, dissolved organic nitrogen (DON) concentrations were similar, leading to significantly (P-value<0.05, t-test) higher C:N ratio (DOC:DON) in the nSM (Figure 1H, I). This is consistent with previous studies suggesting high DOC release from nitrogen-starved *Prochlorococcus*, potentially due to "overflow metabolism" as the cells continue to fix carbon without being able to form new biomass, thus releasing carbon-rich molecules (*7*, *8*, *26*, *52*, *53*). In contrast, dissolved DNA was measurable only in the vSM (Figure 1F), likely representing released phage particles. Indeed, the vSM contained infective phages (Figure S2).

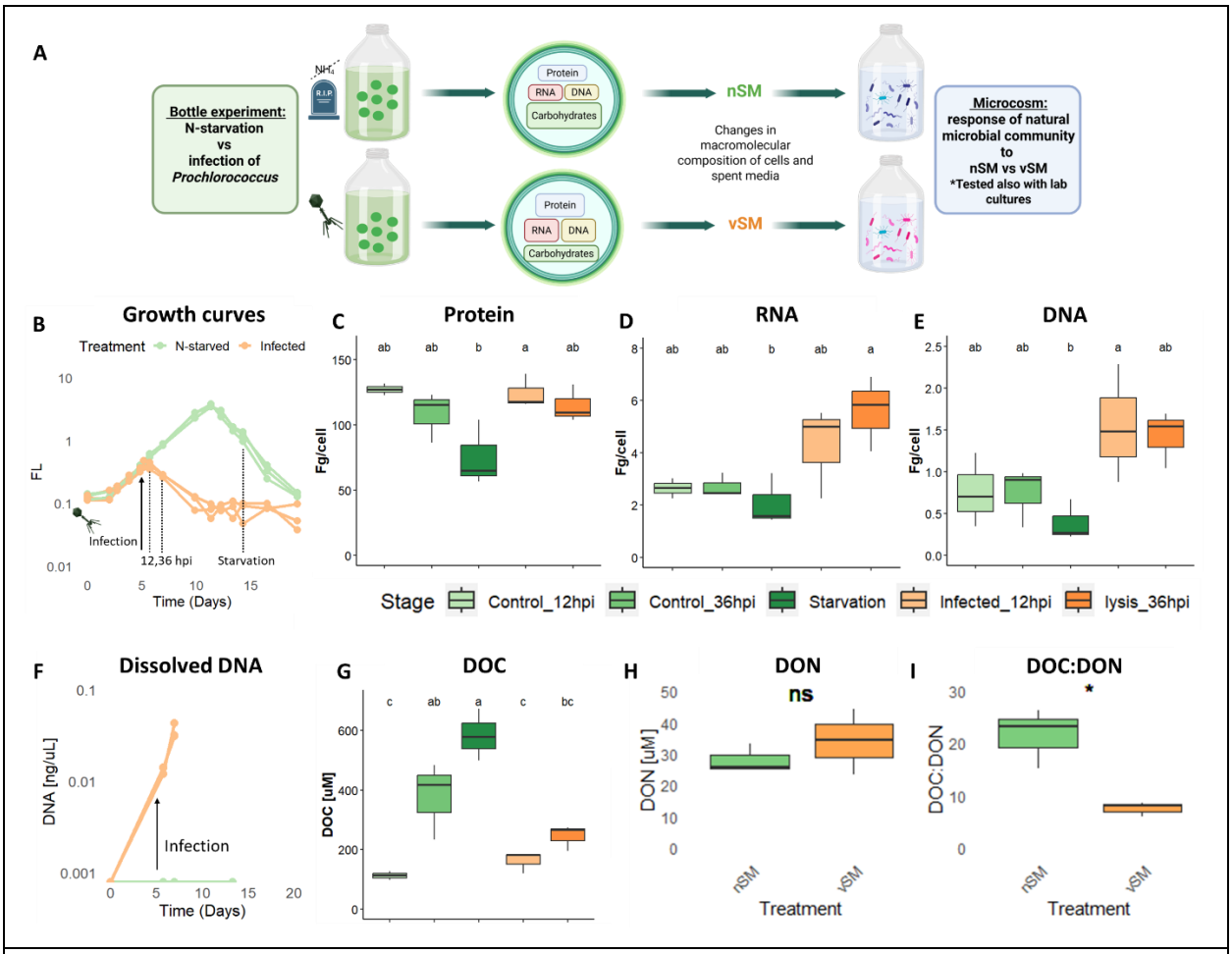

Figure 1. **Effect of nitrogen starvation and phage infection on the macromolecular composition of *Prochlorococcus* MED4**. (A) Illustration of the experimental set-up. (B) Growth curves of N-starved (green) and infected (orange) *Prochlorococcus* – fluorescence, a proxy for cells numbers. (C) Protein quotas in *Prochlorococcus* cells. (D) RNA quotas. (E) DNA quotas. (F) Dissolved DNA nSM (green) and vSM (orange). (G) Dissolved organic carbon (DOC) concentrations. (H) Dissolved organic nitrogen (DON) in nSM and vSM. (I) DOC:DON ratio in nSM and vSM. Box-Whisker plots show the interquartile range (25th–75th percentile) of the data set. The horizontal line within the box represents the median value (N=3). The different letters above the box plots (C, D, E, G) indicate statistically significant differences among the treatments (one-way ANOVA and post-hoc Tukey test, $p < 0.05$). Asterisks above the box plots (H, I) indicate statistically significant differences between treatments based on t-tests ($p < 0.05$). Abbreviations: hpi = hours post infection; nSM- spent media following nitrogen starvation; vSM - viral spent media.

DOM from N-starved and infected Prochlorococcus has distinct effects on bacterial activity and dark carbon fixation in natural microbial communities

We next added nSM and vSM to natural microbial communities from the Eastern Mediterranean Sea (EMS) in two separate experiments, one during autumn, when the water column was highly stratified and oligotrophic (Figure S3A-C), and another during spring, when the water column was mixed and nutrients concentrations were much higher (Figure S3D-F). The amendments contained equal amounts of DOC (25 μM, a concentration used in previous studies (*30*, *54*)), as well as NH_4^+ and PO_4^{2-} to make sure the microbial communities were not nutrient-limited and could thus respond to the potentially different compositions of organic carbon sources.

During both autumn and spring, the addition of vSM led to a significant (*P*-value<0.05, ANOVA) increase in total cell counts compared to the control where only inorganic nutrients were added, whereas the addition of nSM did not result in a significant change (Figure 2A, Figure S4A). Further examination of the flow cytometry scattergrams indicated that the differences between the nSM and vSM in both experiments were primarily due to a higher increase in the number of low nucleic acid (LNA) cells in response to vSM (*P*-value<0.01, ANOVA, Figure S4C). LNA cells, characterized by reduced fluorescence intensity, small cell size, and compact genomes, are highly abundant in oligotrophic oceans, yet their precise identity remains uncertain (*55*). In this study, the LNA population exhibited a larger increase in the intensity of Sybr-green staining in the vSM (*P*-value<0.001, ANOVA, Figure S4F, G). Assuming that the intensity of Sybr-green staining is related to the nucleic acid content of the cells, this might suggest that LNA cells increased both in abundance and activity (*56*), primarily in response to vSM. Bacterial production (BP), measured as the incorporation of radioactive leucine, also increased significantly during spring in response to the vSM than the nSM (*P*-value<0.001, ANOVA, Figure S5D, BP measurements during autumn

were unreliable). Taken together, these results, including increased total cell counts, higher abundance and activity of LNA cells, and elevated bacterial production, suggest that viral lysate elicits faster growth and more heterotrophic activity compared to nSM. This is consistent with experiments performed in the South China Sea with the lysates of P-HM2 and two other phages compared with spent media from exponentially-growing *Prochlorococcus* (*22*).

In addition to BP, we also measured dark carbon fixation (DCF), the incorporation of CO_2 into biomass without light energy. DCF can be performed by chemoautotrophs, which use inorganic electron donors such as CO_2 or H_2, or by heterotrophic bacteria which use organic matter as a source of energy (see details below). Heterotrophic CO_2 fixation is increasingly recognized as a significant and previously overlooked contributor to CO_2 assimilation in marine environments, occurring not only in the deep, dark ocean but also in shallower waters (*33*, *57–62*). Intriguingly, we observed a significant increase in DCF in the nSM but not vSM during both autumn (*P*-value<0.001, ANOVA, Figure 2B, C) and spring (*P*-value<0.01, ANOVA, Figure S5B, C) experiments, reaching in our experimental incubations levels comparable to photosynthesis in the oligotrophic Mediterranean and Red Seas (see Supplementary text 1).

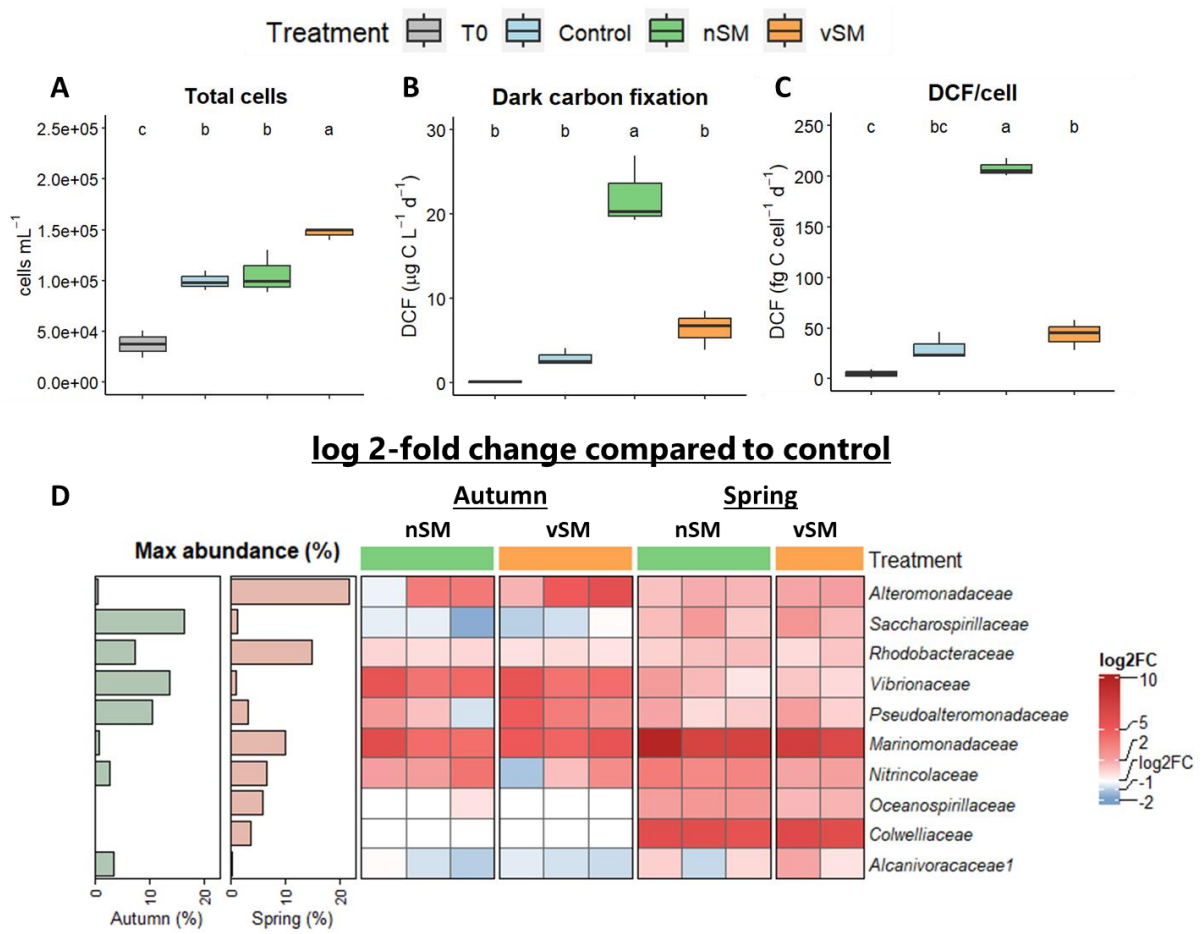

Figure 2. **Spent media from N-starved and infected *Prochlorococcus* differently affect natural microbial community activity and structure.** (A) Total cells count. (B) Dark inorganic carbon fixation (DCF). (C) Per-cell DCF. Box-Whisker plots show the interquartile range (25th–75th percentile) of the data set. The horizontal line within the box represents the median value (N=3). The different letters above the box plot indicate statistically significant differences among the treatments (one-way ANOVA and post-hoc Tukey test, $p < 0.05$). (D) Heatmap showing the $\log_2$ fold change in relative abundance of the top bacterial families enriched in the nSM and vSM compared to the control, based on 16S rRNA sequencing. Each column is an experimental replicate, and each row is a family for which at least one replicate showed a relative abundance above 1% and a fold change greater than 2 compared to the nutrient-only control. The bar-plots on the left of the heatmap show maximum relative abundance in nSM or vSM in the autumn (green) and spring (pink). For the full bar-plot of the community structure and more discussion please see Figure S6 and Supplementary text 2. Abbreviation: DCF – dark carbon fixation; nSM- spent media following nitrogen starvation; vSM - viral spent media.

16S amplicon sequencing reveals no specific clades enriched in the nSM that could be associated with DCF

We expected the differences in the functional response to nSM and vSM to be mirrored by differences in the community structure, as assessed by amplicon sequencing of the 16S rRNA (which is affected by both relative organism abundance and activity, i.e., number of ribosomes). Specifically, we expected to identify organisms (represented by Amplicon Sequence Variants, ASVs) which exhibit a higher increase in relative abundance in response to nSM than to vSM compared to the no-DOM control. Such ASVs would be good candidate organisms responsible for the increased DCF. However, while the nSM and vSM differed from the nutrient-only controls in both autumn and spring experiments (Figure S6), no ASVs were specifically enriched in the nSM (Figure 2D). Several bacterial families increased in relative abundance in both treatments compared to the controls, including (during autumn) *Vibrionaceae*, *Pseudoalteromonadaceae* and *Rhodobacteraceae* (Figure 2D, Figure S7). During spring, *Alteromonadaceae* rather than *Pseudoalteromonadaceae* increased significantly in both treatments (Figure 2D). These results are in agreement with previous experiments where spent media from *Prochlorococcus* was added to natural communities (*22*, *54*, *63*).

During the Autumn experiment we sequenced also 16S rDNA amplicons (Figure S8), which reflects relative abundance and not activity. *Pseudoalteromonadaceae* and *Vibrionaceae* increased significantly in relative abundance in both rDNA and rRNA amplicons, suggesting rapid growth in response to nSM and vSM. In contrast, the relative abundance of *Rhodobacteraceae* increased only in the rRNA and not the rDNA, suggesting increased activity without necessarily a concomitant increase in cell numbers. The specific *Vibrionaceae* and *Rhodobacteraceae* ASVs responding during autumn and spring were not identical, suggesting temporal differences in the

fine-scale community structure or function between the two seasons (Figure S6). Analysis of 18S rRNA sequencing from the autumn experiment revealed no significant changes in eukaryotic community structure (Figure S9).

Identifying clades with the capacity for DCF using metagenomics

Since the 16S and 18S amplicon sequencing was not able to highlight microbial clades responsible for the increased DCF, we next searched for relevant pathways (and, subsequently, individual genes) in metagenomes from the nSM, vSM and control incubations. Broadly speaking, *autotrophic* CO_2 fixation is mediated by pathways such as the reverse tricarboxylic acid (rTCA) cycle or the Wood-Ljungdahl pathway (*64*). In contrast, the primary process in *heterotrophic* CO_2 fixation is anaplerosis, the replenishment of tricarboxylic acid (TCA) cycle intermediates such as oxaloacetate and malate (see below). Autotrophic CO_2 fixation pathways in prokaryotes (KEGG pathway ko00720) were enriched in both the nSM and vSM compared to no-DOM controls, but this was not statistically significant, and no clear difference was observed between the nSM and vSM (Figure S10). This suggests that chemoautotrophy is not the main process responsible for the observed DCF. Heterotrophic CO_2 fixation, which is composed of various individual genes (see below), lacks a dedicated KEGG pathway, and therefore could not be assessed at the pathway level. However, the nSM metagenome was enriched in pathways related to carbohydrate utilization (e.g., the tricarboxylic acid (TCA) cycle and pyruvate metabolism), lipid metabolism (fatty acid metabolism) and amino acids synthesis (e.g., valine, leucine, and isoleucine biosynthesis) (Figure 3). We interpret these results as evidence that C-rich molecules such as carbohydrates and lipids were more abundant in the nSM compared with the vSM, consistent with the higher DOC:DON ratio.

If indeed carbon-rich molecules are major components of the nSM, organisms utilizing them as resources would likely need to produce their own nitrogen-rich building blocks such as amino acids and nucleotides from TCA cycle intermediates, rather than taking them up from the environment. In this case, the cell needs to compensate for flux diverted from the TCA cycle into biosynthesis by using one or more of six specific anaplerotic reactions, four of which also include a CO_2 fixation step (Figure 4A, (*60*)). Genes encoding the CO_2 fixing enzymes phosphoenolpyruvate (PEP) carboxylase (PEPC), PEP carboxykinase (PEPCK) and malate dehydrogenase (MDH) were relatively abundant in the metagenomes, whereas pyruvate carboxylase (PC) was less common (Figure 4B). Overall, there was no significant difference in the abundance of these genes between the nSM, vSM and controls (Figure 4B), yet in each treatment the sequences of these genes primarily originated from different bacterial orders (Figure 4C). For example, genes encoding PEPCK and MD from *Vibrionales* and *Rhodobacterales*, respectively, were enriched in the nSM (~1.5-3.5 and ~2-4.5-fold change compared to vSM), suggesting these clades might be involved in the observed DCF. In contrast, PEPC, PC and MD from *Pelagibacterales* were enriched in the vSM (~1.4-2.8-fold change), as were PEPC from *Pseudoalteromonadales* (~4-fold change), positioning these clades as less likely candidates for the observed DCF. Similar results were observed also for genes encoding enzymes in the glyoxylate shunt (malate synthase and isocitrate lyase), an anaplerotic process that does not include a CO_2 fixation step (Figure 4A). Genes encoding other heterotrophic CO_2 fixing enzymes, such as those involved in leucin utilization or biotin production, were less common in the metagenomes (Figure 4B).

Analysis of metagenome-assembled genomes (MAGs) provided further support for hypothesis that heterotrophic, rather than autotrophic, processes were involved in the DCF, as pathways encoding

the former were more commonly found and more complete within MAGs (Figure S11). Anaplerotic genes were present at varying levels of completeness across all MAGs, with *Rhodobacteraceae* MAG MED-G52 possessing all of the 4 CO_2-fixing genes (Figure 5). However, the MAGs also further highlighted that there are other clades (primarily alpha and gamma proteobacteria and flavobacteria) that have the genetic potential to perform DCF.

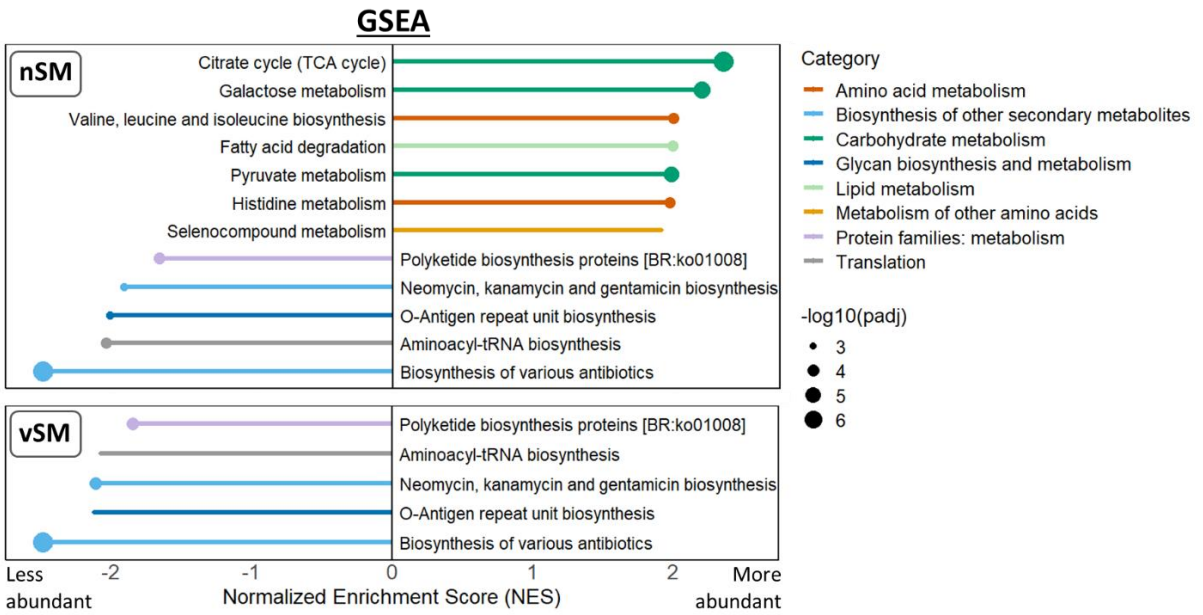

Figure 3. **Gene set enrichment analysis (GSEA) of differentially expressed genes in nSM and vSM**. Only statistically significant pathways (adjusted *p*-value < 0.05) are shown. The size of the bars represents the normalized enrichment score (NES). The size of the points represents the adjusted *p*-value. For expanded GSEA results see Figure S10.

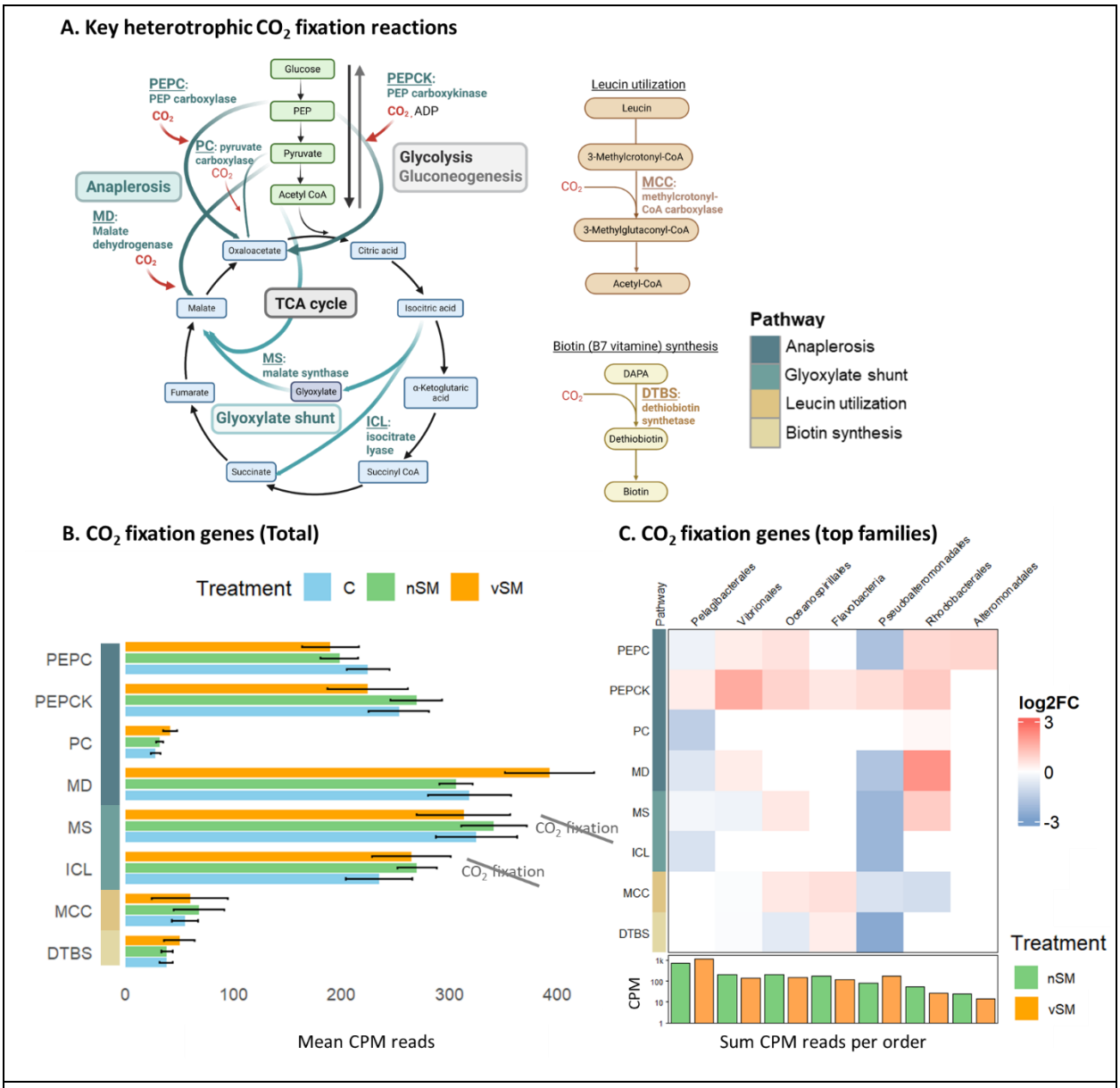

Figure 4. Metagenome analysis for CO_2 fixation pathways. (A) Diagram illustrating key heterotrophic CO_2 fixation reactions, along with the TCA, glyoxylate shunt and gluconeogenesis. DAPA: 7,8-diaminononanoate. Scheme was modified from Amano et al. (*58*). (B) Total normalized reads (CPM)) for key enzymes associated with heterotrophic CO_2 fixation. (C) Heatmap for average (N=3) fold change of nSM relatives to vSM reads for major heterotrophic taxa, which exhibited the highest relative abundance of discussing genes (based on CPM reads, Figure S12). Bottom bar plots showing sum CPM reads of all genes for each bacterial family in nSM (green) and vSM (orange). Abbreviations: PEPC - phosphoenolpyruvate (PEP) carboxylase; PEPCK - PEP carboxykinase; PC – pyruvate carboxylase; MDH - malate dehydrogenase; MS – malate synthase; ICL – isocitrate lyase; MCC - methylcrotonyl-

CoA carboxylase; DTBS - dethiobiotin synthetase. Although ICL and MS have anaplerotic role, they are not involved in CO_2 fixation – for more details see Supplementary text 3.

Cultured Rhodobacterales and Alteromonadales strains perform higher DCF in response to nSM compared to vSM

The metagenomic analysis highlights *Rhodobacterales* and *Alteromonadaceae* (as well as *Oceanospirillales* and *Vibrionales*) as orders potentially involved in the higher DCF in nSM treatment, and *Pseudoalteromonadales* and *Pelagibacterales* as relatively abundant clades less likely to do so (Figure 4C). To begin testing these hypotheses, six laboratory cultures, representing the major orders found in our metagenome analyses, were starved for carbon to simulate oligotrophic conditions followed by the addition of nSM and vSM (see materials and methods). Two of the strains, *Alteromonas mediterranea* strain DE (*Alteromonadales*) and *Marinovum* strain HOT5_F3 (*Rhodobacterales*), exhibited elevated per-cell DCF in the nSM (Figure 5), reminiscent of the observations in the field experiments (Figure 4C). None of the strain exhibited significantly higher DCF in response to vSM. Bacterial production also increased more in *Alteromonas* in response to nSM compared to vSM, and thus the DCF could, in principle, represent stronger overall growth. In contrast, only DCF increased in *Marinovum*, suggesting a specific metabolic response that is not coupled with growth, at least not in the time-frame of the experiment. This is similar to the response of the *Rhodobacterales* in the two experiments with natural microbial populations (Figure 3C).

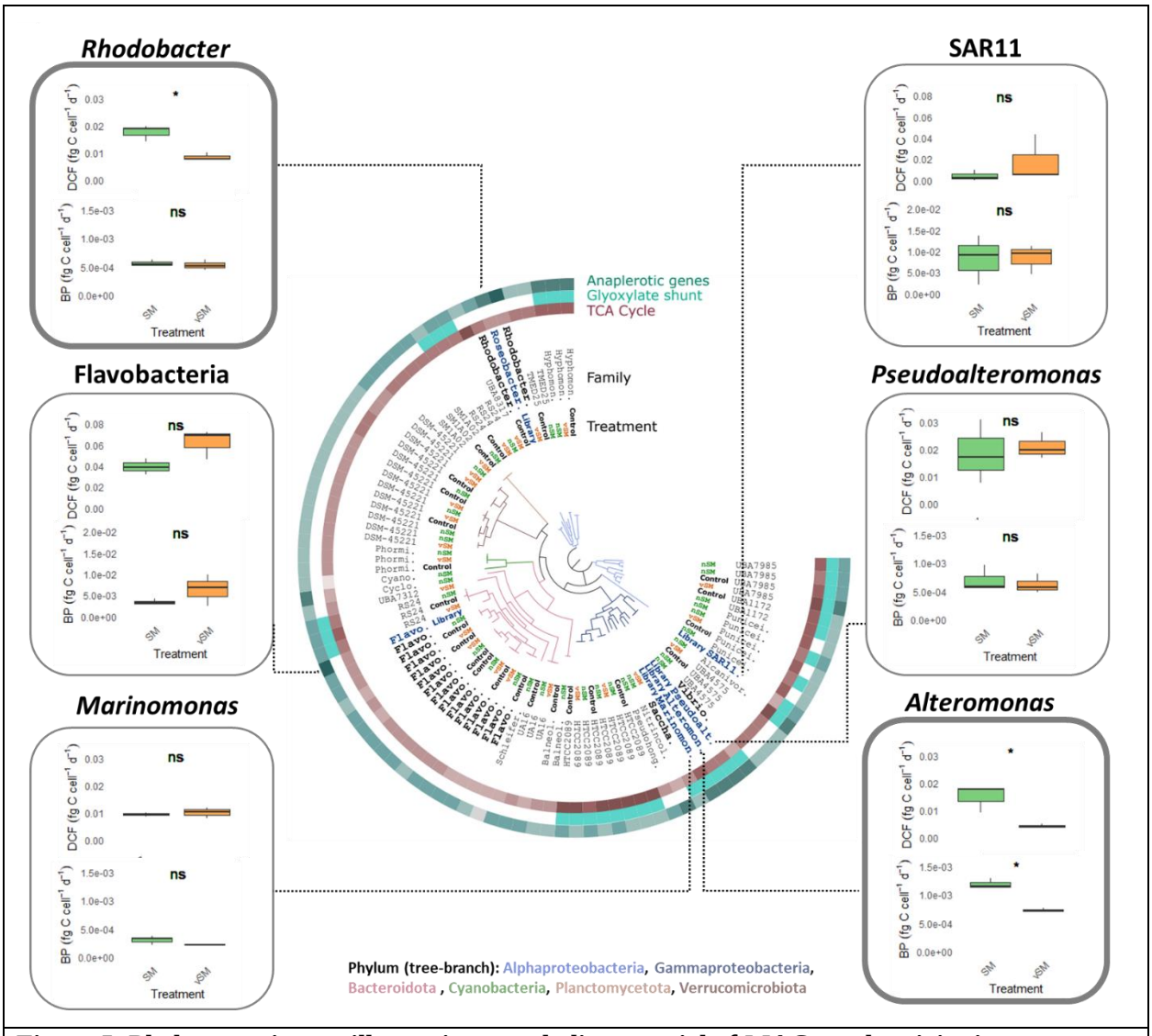

Figure 5. **Phylogenomic tree illustrating metabolic potential of MAGs and activity in response to vSM and nSM of representative laboratory taxa**. The outer rings indicate the presence of genes related to the TCA cycle, glyoxylate shunt, and anaplerotic pathways. Taxa are further annotated by bacterial family (inner ring) and treatment condition (control: black, nSM: green, vSM: orange). Bacterial taxa discussed in Figure 4C are highlighted in bold, and genomes derived from laboratory cultures are shown in blue. Boxplots adjacent to the tree illustrate per-cell dark inorganic carbon fixation (DCF) and bacterial production (BP) rates (in fg C cell^{-1} d^{-1}) for selected laboratory strains that belong to the orders displayed in Figure 4C. An asterisk (*) denotes statistically significant results (p-value < 0.05), determined by a paired t-test with Bonferroni correction. Note the distinct Y-axis scales for *Flavobacteria* and SAR11 compared to other strains, likely attributable to their lower cell counts as measured by flow cytometry (Figure S13A).

Abbreviations for the family level: Alcanivor. – *Alcanivoracaceae*; Alteromon. – *Alteromonadaceae*; Balneol. – *Balneolaceae*; Cyano. – *Cyanobiaceae*; Cyclo. – *Cyclobacteriaceae*; Flavo. – *Flavobacteriaceae*; Hyphomon. – *Hyphomonadaceae*; Marinomon. – *Marinomonadaceae*; Nitrincol. – *Nitrincolaceae*; Phormi. – *Phormidesmiaceae*; Pseudoalt. – *Pseudoalteromonadaceae*; Pseudohong. – *Pseudohongiellaceae*; Punicei. – *Puniceispirillaceae*; Rhodobacter. – *Rhodobacteraceae*; Saccha. – *Saccharospirillaceae*; Schleif. – *Schleiferiaceae*; Vibrio. – *Vibrionaceae*.

Abbreviations for the library strains (in blue): Alteromon. – *Alteromonas mediterranea* DE; Flavo. – *Formosa agariphila* KMM; Marinomon. – *Marinomonas mediterranea* MMB1; Pseudoalt. – *Pseudoalteromonas haloplanktis* TAC; Roseobacter. – *Roseobacteraceae Marinovum* HOT5_F3 (order of *Rhodobacterales*); SAR11 - Candidatus pelagibacteraceae St. HTCC1062 (refer to Table S1 for full details).

Summary and Conclusions

There are many ways microbial cells can die in the oceans. In laboratory cultures, whether *Prochlorococcus* MED4 dies due to phage infection or nitrogen starvation affects its biochemical structure, and the composition of DOM released upon death. In turn, these changes can have cascading effects on the microbes in the surrounding seawater, including shifts in bacterial community activity, metabolism, structure and function. DOM released through viral lysis increased overall heterotrophic community production, in agreement with a recent study (*65*), but we show for the first time that DOM from nutrient-starved cells increases heterotrophic CO_2 fixation (Figure 6).

In theory, phytoplankton biomass provides a "balanced meal" of building blocks (amino acids, nucleotides) and energy-rich molecules (carbohydrates, lipids) for heterotrophic bacteria (*8*, *54*). However, the biochemical composition of the “meal” can change in response to different forms of death. Under nutrient starvation, phytoplankton like *Prochlorococcus* may shift towards producing and releasing excess carbon-rich metabolites, such as carbohydrates, through a process known as "overflow metabolism" (*6*, *53*, *66*). Previous studies have shown that a significant portion of the

carbohydrates released by *Prochlorococcus* are carboxylic acids such as pyruvate, glycolate, acetate and citrate (~4-20%, (*6*, *25–28*, *53*, *66*)). These carboxylic acids either feed directly into the TCA cycle or are components of the cycle itself. We propose that such molecules (or their polymeric forms, e.g. lipids) comprise a larger part of the DOM released during starvation compared with phage lysis. We also propose that heterotrophic bacteria will need to employ anaplerotic reactions to enable them to utilize these carbon-rich molecules as resources for both energy and as backbones for biosynthesis of proteins and nucleic acids, e.g. using inorganic nitrogen sources. In support of this hypothesis, the DOC:DON ratio of the nSM was higher than that of the vSM, and pathways such as the TCA cycle, pyruvate metabolism, and fatty acid degradation were enriched in the community responding to the nSM (Figure 6).

Additionally, two of the clades shown to respond to nSM by growth and/or DCF, *Alteromonadales* and *Rhodobacterales*, respond in the lab and in the field to additions of organic acids, monosaccharides and disaccharides (*30*, *67–70*). Amano et al. (*58*) also demonstrated that *Alteromonas* DE exhibits higher DCF rates on glucose compared to alanine, further supporting our hypothesis that carbon-rich DOM contributes to elevated DCF. Both of these clades are often associated with phytoplankton blooms and exudates, particularly those of cyanobacteria (*71*, *72*). Taken together, these results, as well as previous studies, suggest an important role for these bacterial clades in anaplerotic CO_2 fixation in the oceans (*58*, *70*, *73*, *74*).

In contrast to nitrogen starvation, cyanophage infection has been shown to increase the release of nitrogen-rich compounds like amino acids (*1*, *22*). This suggests that DOM released by phage infection, and, potentially, phage themselves, are a source of bioavailable nitrogen, and potentially also other limiting nutrients such as phosphorus (*75–77*). We propose that the larger increase in *Pseudoalteromonadaceae* abundance observed following vSM exposure in the autumn experiment

was due to vSM's nitrogen-rich composition, since cultured representatives of this clade demonstrated preferences for peptides in laboratory cultures and field incubations (*30*, *67*). It is currently unclear whether the heterotrophic bacteria utilize nitrogen-rich lysate molecules such as cellular proteins or nucleic acids, or whether they take up and metabolize the phage themselves.

Our findings align with a global ocean metatranscriptomic study highlighted the ubiquitous expression of anaplerotic and glyoxylate shunt genes, often exceeding those involved in chemoautotrophy (*58*). If, indeed, a fraction of this heterotrophic CO_2 fixation is due to the presence of organic matter released due to nutrient starvation, this could have important consequences for understanding the cycling of dissolved organic carbon pools in the ocean. The relative contribution of different forms of death - grazing, phage infection and nutrient starvation – to the overall mortality of *Prochlorococcus* is still not well known (*9–12*). However, it is intriguing that in the oligotrophic Gulf of Eilat, higher DCF rates occurred during the oligotrophic summer (~12% vs. ~7.5% in winter), supporting the link between nutrient scarcity and increased DCF (*61*). It is also important to note that the increase in the released DOC:DON ratio does not necessarily require cell death, but can also occur as a result of overflow metabolism where fixed carbon is released when there is not enough N/P/Fe to fuel cell growth (*78*). These processes (overflow metabolism and/or nutrient starvation) could be important processes responsible for increased DOC in the subtropical gyres (*79*). Taken together, these results provide additional motivation to determine to what extent there exists a close coupling between specific forms of mortality, the release of DOM and its subsequent metabolism, the temporal succession of microbes in the sea (e.g. the succession of heterotrophic bacteria during phytoplankton blooms) and biogeochemical cycles.

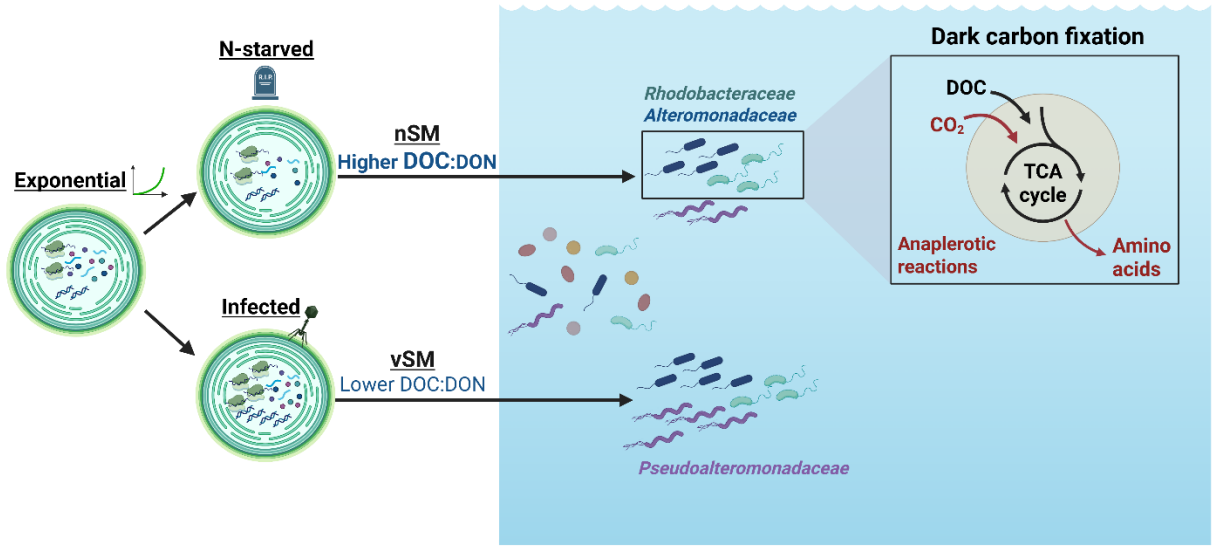

Figure 6. **Summary illustration of experimental observations and suggested mechanism**. Phage infection resulted in increased RNA and DNA quotas, whereas nitrogen-starved cells showed decreased protein quotas compared to logarithmic growth. Starved cells released more DOC concentration, while infected cells released more virions, found as dissolved DNA in the viral spent media (vSM). Addition of vSM resulted in increased total cells count and bacterial productivity. Addition of nSM increased dark inorganic carbon fixation (DCF) in both microcosm experiments and cultures of *Rhodobacterales and Alteromonadales*, which were also observed in the 16S rRNA analysis. Metagenomic analysis revealed an enrichment of pathways in the nSM treatments, including the TCA cycle, pyruvate metabolism, and phospholipid degradation.

Materials and Methods

***Prochlorococcus* bottle experiment: experimental setup and samples collection.** Triplicate bottles containing 750 mL of *Prochlorococcus* MED4 were grown in low-nitrogen media (lowN, (*43*)): Mediterranean sweater (MSW) supplemented with 200µM NH_4, 50µM PO_4 and 10,000X trace metals (*80*). After 5 days, half of the bottles were inoculated with cyanophage P-HM2 at MOI of 2:1. P-HM2 is a T4-like myovirus with a latent period of approximately 5 hours (*22*, *81*). The aim of the experiment was to compare the macromolecular composition of MED4 cells and

lysate under two conditions: (1) nitrogen starvation and (2) phage-induced cell lysis. This allowed us to test the hypothesis that protein and RNA quotas in infected cells would increase due to elevated virion production.

Cells were infected on day 5, during early-to-mid logarithmic growth. Sampling occurred at three timepoints: T1 (~12 hpi, following at least one round of infection), T2 (~36 hpi, following several infection cycles), and T3 (uninfected samples only) captured the mid-decline stage for the N-starved culture (Figure 1B). Samples for protein, RNA and DNA quantification were collected at each timepoint in triplicate or duplicate (for proteins) by filtering ~50 mL on 0.7 µm GF/F, preserved in lysis buffer (40 mM EDTA, 50 mM Tris, pH 8.3, 0.75 M sucrose), and stored at -80˚C until further analysis. Flow cytometry samples were fixed with a final concentration of0.125% glutaraldehyde for 10 minutes, frozen, and stored at -80˚C until counted using BD Canto II flow-cytometer. Additionally, samples for measuring NH_4, PO_4, DOC and dissolved protein, RNA and DNA (as described below) were taken from the media after filtration (0.2 µm polycarbonate filters) and stored at -20˚C. All remaining lysate from T_2 (infected) and T_3 (uninfected) was retained at -20˚C for the microcosm experiment.

Cruise and microcosm experimental set-up. Spent media from nitrogen-starved (nSM) and viral-infected (vSM) *Prochlorococcus* was introduced into surface seawater collected from the Eastern Mediterranean Sea. This experiment was conducted twice: once in autumn (November 2022) and once in spring (March 2024). Seawater for both experiments were collected at station H05 (32.99°N, 34.50°E), an open ocean site, from a depth of 25m. Seawater for the autumn experiment were sampled on November 7, 2022. Concentration of nutrients were 0.03 µM for total N (NO_2 and NO_3) and below limit of detection for phosphate (Figure S3B, C). Depth of the deep chlorophyll maximum (DCM) was ~75m and was mostly comprised of small phytoplankton

fraction, as suggested by the fractionated chlorophyll extraction (Figure S3A). Seawater for the spring experiment were sampled on March 28, 2024 during an IOLR transect cruise (H51). Concentration of chlorophyll (approximately 0.1 µg/L) and nutrients (approximately 10 nM for PO_4 and ~0.25 µM for NO_2 and NO_3) were higher than November (Figure S3D-F), consistent with expected seasonal patterns.

The experiment included 3 treatments: (1) "nSM", amended with spent media from N-starved cells (T3 in the bottle experiment), (2) "vSM", amended with lysate from infected cells (T2 in the bottle experiment) and a control amended only with inorganic N and P to isolate the impact of organic carbon composition. To ensure that observed effects were due to differences in DOC composition rather than quantity, final DOC concentration was set to 25 µM. Additionally, NH_4 and PO_4 were added at a final concentration of 15 µM and 10 µM, respectively - levels corresponding to the highest concentrations measured in the *Prochlorococcus*-derived DOM from either experimental replicate. Triplicate bottles of 4L (autumn) and 400mL (spring) from each treatment were incubated in dark for 24 hours. In both experiments, samples for cells count, bacterial productivity and DCF were taken at T_0 from the seawater prior to the experimental setup and at end of the incubation (T_{24}). In addition, samples for both 16S rRNA and rDNA and 18S rRNA were collected in the autumn, and for 16S rRNA in the spring.

Lab-cultures experiment with heterotopic bacteria. Bacterial cultures were revived in 2 mL of marine broth (MB) at 26°C for 48 hours in 12 mL sterile growth tubes, followed by several transfers to induced carbon starvation: 500µl of cultures were then transferred to 5mL ProMM medium and incubated for 72 hours at 26°C, followed by an additional similar transfer and 48-hours incubation at 22°C. Subsequently, 5mL of cultures were transferred to 20 mL sterile seawater (SW) and incubated at 22°C for 24 hours in sterile glass tubes. SAR11 HTCC1062 was

cultured individually in low-nutrient media supplemented with 80 µM pyruvate, 40 µM oxaloacetate, 40 µM taurine, or 50 µM glycine as the sole carbon source. Cultures were grown for 10 days until reaching the late exponential phase, indicating carbon source depletion. SAR11 cells were counted using Guava EasyCyte Plus flow cytometer, and all other cultures were counted using Cytoflex flow cytometer. Bacteria (final concentration of 10^5, similar to seawater cell counts) were added to sterile SW (final volume of 80mL in 300mL bottles) supplemented with NH_4 and PO_4 and either nSM or vSM at microcosm-equivalent concentrations. Samples were incubated in darkness at 22°C for ~20 hr, after which samples for FCM analysis were collected, and radioactive incubations (4 hr) for BP and DCF measurements were initiated.

Plaque assay for quantifying viable phages. The plaque assay of phage P-HM2 was used to quantify viable phages for infecting *Prochlorococcus* MED4. *Alteromonas* DE served as a helper bacterium (*82*) for plating *Prochlorococcus* on low melting point (LMP) agarose (Invitrogen, UltraPure LMP agarose, cat no. 16520-100) plates. *Alteromonas* DE was prepared by centrifuging 1ml of overnight culture growing in ProMM (*82*) at 8000 RPM for 2 minutes, resuspending in 1ml of Pro99, and repeating the washing step twice before final resuspension in 1ml Pro99. All solutions were prepared using Milli-Q water (Millipore system). Na_2SO_3 stocks (1M concentration) was freshly prepared on the day of plating and sterilized using a 0.2µm syringe filter. A 0.35% LMP agarose solution was prepared by adding 0.35g of LMP agarose per 100ml of autoclaved MSW and microwaving to dissolve. After cooling to ~33ºC, nutrients were added to Pro99 medium (800µM NH_4, 50µM PO_4, 10,000X trace metals) supplemented with 1M Na_2SO_3. The agar solution was allowed to cool to ~30ºC before use. Phage lysate was serially diluted (10^{-1} to 10^{-6}) in Pro99 before plating. For plating, 2.7 mL of *Prochlorococcus* (~10^8 cells), 100µl of *Alteromonas* (~10^6 resuspension in Pro99) and 200µl of diluted lysate were added and mixed by

pipetting. Then, 12ml of 0.35% LMP agarose was added to the opposite side of the plate, and the plates were mixed gently before agar was solidified. Plates were allowed to dry for 1 hour, sealed with parafilm, and incubated at ~22ºC on a net to prevent direct contact with the glass tray, reducing heating and steam accumulation. Plaques were typically observed within a week.

Measurements of bulk protein, RNA and DNA. Samples for protein, RNA and DNA were filtered on 0.7 μm GF/F filters and stored at -80°C until analysis. Proteins were extracted by incubating the samples with lysis buffer at 37˚C for 30 minutes, followed by 10 min of sonication in a water bath (Ultrasonic Cleaner AC-120H), and quantified using the bicinchoninic acid (BCA) assay (*83*). RNA was isolated from the filter using Trizol extraction (*84*), and DNA using Phenol-Chloroform (*85*). The concentration of both RNA and DNA was determined with the Qubit™ RNA HS Assay Kit and Qubit™ dsDNA HS Assay Kit, respectively.

Measurements of NH_4, PO_4, DOC and DON in nSM and vSM. Samples for NH_4 and PO_4 were filtered through 0.2 μm polycarbonate filters and stored at -20°C until analysis. Prior to measurements, samples were diluted 4-fold in DDW to reduce the salt level. NH_4 was measured using an HI 96715 meter (Hanna instrument), and PO_4 using Phosphate Colorimetric Assay Kit (Catalog Number MAK030). Samples for dissolved organic carbon (DOC) and total nitrogen (TN) were filtered through 0.2 μm polycarbonate filters. DOC samples were collected into cleaned, pre-combusted, acid washed (10% HCL) 40ml vials, added with 20μL of 36% HCL to remove dissolved inorganic C before preservation at 4ºC under dark. DOC was measured a few days later via InnovOx Analyzer (Serial Number 1051, Version 03.10.017). TN samples were collected into cleaned 50ml falcon tubes and preserved at -20ºC until measured photometrically using a Foss Analytical FIAstar 5000 115 Analyzer with DDW detector and a common standard for TN (AN

5202D, DIN EN ISO 117 13395, ISO 11905). Dissolved organic nitrogen (DON) concentrations were calculated by subtracting ammonium concentrations from the total nitrogen values.

Bacterial productivity. Bacterial productivity (BP) was estimated using the ^{3}H-leucine incorporation method (*86*) as detailed by (*87*). Triplicate 1.7 mL seawater samples were incubated with ^{3}H-leucine (10 nmol 'hot' leucine L^{-1}) for 4 hours room temperature in the dark immediately after sampling. The reaction was stopped by adding 100 µL of trichloroacetic acid (TCA), and the samples were processed at the end of the cruise following the micro-centrifugation protocol (*86*). 1 mL of scintillation cocktail (ULTIMA-GOLD) was added to each sample before measurement using a TRI-CARB 2100 TR (PACKARD) scintillation counter.

Dark inorganic carbon fixation. Dark inorganic carbon fixation (DCF) was measured using the ^{14}C incorporation method (*88*), with few modifications (*89*), as described by Reich et al. (*87*). Triplicate 50 mL samples were spiked with 50 µL (5 µCi) of $NaH^{14}CO_3$ and incubated for 24 hours in the dark at ambient temperature. After incubation, samples were filtered through 0.7 µm GF/F filters under low vacuum pressure, rinsed with filtered seawater, and treated with 50 µL of 32% HCl to remove excess ^{14}C-bicarbonate. Filters were then incubated overnight before adding 5 mL of scintillation cocktail, and radioactivity was measured using a TRI-CARB 2100 TR scintillation counter.

16S RNA and DNA extraction, DNA digestion, and cDNA synthesis. The bacterial community structure and activity were assessed through 16S and 18S rRNA and rDNA sequencing. For each incubation bottle, 1–2 L of seawater was filtered onto 0.2 µm filters, preserved in lysis buffer, and stored at −80°C until extraction. RNA and DNA were extracted using the NucleoSpin RNA Stool and the PureLink™ Genomic DNA Mini Kit, respectively, according to the manufacturer's

instructions. RNA extraction included DNase treatment, followed by reverse transcription into cDNA using the iScript cDNA Synthesis Kit.

16S and 18S rRNA and rDNA sequencing. 16S rRNA and rDNA sequencing was conducted using primers 515F and 926R (*90*), targeting ~400 bp products. For 18S rRNA, primers Euk_1391F and EukBR were used, targeting ~200 bp products. Sequencing protocols are described in detail in Givati et al. (*30*). Briefly, amplicons were generated using a two-stage PCR protocol, and libraries were sequenced on an Illumina MiSeq platform (V3 chemistry, 2 × 300 bp reads) with a 15% phiX spike-in. Library preparation and sequencing were performed at the Genomics and Microbiome Core Facility, Rush University, IL, USA.

16S rRNA and rDNA sequence analysis. All sequences of both autumn and spring experiments were analyzed together using the Dada2 pipeline (*91*) and the software packages R (*92*) and Rstudio (*93*), as detailed in Givati et al. (*30*). Forward and backward primers were trimmed, and forward and backward reads were truncated after quality inspections to 230 and 200 bases, respectively. After sequences merging, a consensus length of only between 353 and 366 bases was accepted, discarding ~30% of sequences in the process. Finally, amplicon sequence variants (ASVs) that have less than 100 in total (all samples) were removed, remaining with a total of ~720 ASVs. Silva database version 138 (*94*) was used for taxonomic assignment. All chloroplasts, mitochondria, archaea, eukaryotes, and ASVs without any taxonomic affiliation were discarded from downstream analyses. Full ASVs and taxonomy list of 16S rRNA and rDNA can be found in Supplementary files 1 and 2.

18S rRNA sequence analysis. Sequences were processed using the DADA2 pipeline, following the same approach as for 16S. Forward and backward reads were truncated after quality inspections to 150 and 150 bases. After sequences merging, a consensus length of only between 125 and 175

bases was accepted. Finally, amplicon sequence variants (ASVs) that have less than 100 in total (all samples) were removed, remaining with a total of 368 sequences. Taxonomic classification was carried out in MEGAN6 (v6.24) using BLASTn results, excluding uncultured or environmental sequences. Assignments were made using the LCA algorithm with the MeganMapDB. Parameters included a Top Percent range of 3–10% and a Minimum Score threshold of 75–100. All bacteria, mitochondria, chloroplast, and ASVs without any taxonomic affiliation were discarded from downstream analyses. Full ASVs and taxonomy list of manually curated 18S rRNA can be found in Supplementary file 3.

Metagenomics sequencing. Shotgun metagenomic libraries were prepared using the Illumina Nextera XT DNA Library Preparation Kit. A total of 9 samples were processed for dsDNA shotgun library preparation. Sequencing was carried out on an Illumina NovaSeq X platform using a 2 × 150 bp paired-end protocol. Approximately 900 million clusters were generated per lane on a 25B flow cell.

Metagenomics and MAGs construction. Raw metagenomic reads were first assessed for quality using FastQC (*95*), followed by quality filtering and trimming using the algorithm bbduk (*96*). For *De-novo* assembly, trimmed metagenomes were assembled using Megahit (*97*). For each biological treatment (Control/SM/vSM), we first pooled the replicate libraries and then performed a combined assembly. Gene calls on each of the assembly files were made using (*98*). All the gene-level KEGG Ortholog (KO) functional annotation was performed using KOFamScan (*99*). Gene- and contig-level taxonomic classifications for each assembly were performed using CAT (*100*). Trimmed short reads for each sample were mapped to the corresponding assemblies (contigs/genes) and coverage information was generated using bowtie2 (*101*). All gene- and

taxonomy-level CPM read counts are provided in Supplementary files 4 and 5 (combined) and in Supplementary files 6 to 8 (separated by treatment).

For reconstructing metagenome assembled genomes (MAGs), assembled contigs for each biological condition were separately binned using MetaBat2 (*102*). A quality assessment i.e. degree of genome completeness and contamination of the genome bins or MAGs was performed using CheckM (*103*). Finally, we performed taxonomic classification of the high-quality MAGs (<10% contamination) by comparing with publicly available bacterial and archaeal genomes in the Genome Taxonomy Database (GTDB) using the tool GTDB-tk (*104*). Most of the MAGs had >85% completion (70 MAGs), but few (13 MAGs) had 70-85% completion in an attempt to include more taxa identified in the 16S sequencing. The completeness of metabolic pathways within their genomes was performed via KEGG decoder script (*105*), in which 'anaplerotic genes' includes MD, PEPC, PEPCK and PC. Full list of software and their version is available on Table S2. For detailed MAGs list and assigned KEGGs see Supplementary file 9.

Differential Gene Set Enrichment Analysis (GSEA). Differential Gene Set Enrichment Analysis (GSEA) was performed using the fgsea R package (*106*). Gene sets were defined based on the KEGG pathway database, utilizing a table containing KO IDs, their corresponding functions, and pathway assignments. Analysis was restricted to KO IDs identified in the metagenome and metabolic pathways containing 10 to 500 KOs. GSEA was conducted with 10,000 permutations, using fold-change values as the ranking metric. Gene sets with an adjusted p-value < 0.05 were considered statistically significant.

Phylogenomic tree. A phylogenomic tree was constructed using Anvi'o (v8) (*107*) based on eight universally conserved ribosomal protein genes (*Ribosomal_L1, L2, L3, L4, L5, L6, S7,* and *S8*). For each genome, the best-matching amino acid sequence of each target gene was identified and

extracted. The resulting protein sequences were aligned, concatenated, and used to infer a maximum likelihood phylogeny with FastTree2 under default parameters. The final tree was visualized using Anvi'o's interactive interface. See Table S1 for details on the bacterial genomes.

Statistics. Data pre-processing and statistical analyses were performed using the R statistical programming language (*92*, *93*) and on Linux ubunto20. One-way analysis of variance (ANOVA) and post hoc Tukey test was performed to compare the treatments in lab and microcosms experiments (Figure 2 and Figure 3) using multcompView (*108*) and dplyr (*109*) packages. Paired t-test with Bonferroni correction was used to compare the means between treatments for each bacteria (Figure 6) using the packages tidyverse v1.3.0 (*110*), rstatix (*111*), and ggpubr (*112*). Microbial community differences between treatments in the NMDS plots were statistically assessed by PERMANOVA on Bray-Curtis dissimilarity matrices, with 999 permutations to determine significance using vegan package (*113*). Plots were originated using the ggplot2 package (*114*).

Data availability. All forward and backward sequence reads were uploaded to NCBI under umbrella project accession number PRJNA1291108: PRJNA1287306 (16S rRNA), PRJNA1287330 (16S rDNA), PRJNA1291108 (18S rRNA) and PRJNAXXX (metagenomics).

Acknowledgements: We thank Ximena Dubinsky for help with the BP measurements, Solvig Pinnow and Hans-Peter Grossart for the DON measurements, Eyal Giesler and Edo Bar Zeev for the DOC measurements, Anat Tsemel and Mike Krom for the inorganic nutrient measurements. We also thank Abdiel Lázaro García and Laura Steindler for the SAR11 cultures, and Ankur Naqib, Adit Chaudhary and Stefan Green from the Rush Research Bioinformatics Core for the metagenomic analysis pipeline. This study was supported by the Israel Science Foundation (grant

number 1786/20 to DS) and by the National Science Foundation - United States-Israel Binational Science Foundation (NSFOCE-BSF 1635070 and NSF-BSF 2246707 to DS).

References

1. L. Cai, H. Li, J. Deng, R. Zhou, Q. Zeng, Biological interactions with Prochlorococcus: implications for the marine carbon cycle. *Trends Microbiol.* **32**, 280–291 (2024).

2. S. J. Biller, R. A. Lundeen, L. R. Hmelo, K. W. Becker, A. A. Arellano, K. Dooley, K. R. Heal, L. T. Carlson, B. A. S. Van Mooy, A. E. Ingalls, S. W. Chisholm, Prochlorococcus extracellular vesicles: molecular composition and adsorption to diverse microbes. *Environ. Microbiol.* **24**, 420–435 (2022).

3. S. J. Biller, F. Schubotz, S. E. Roggensack, A. W. Thompson, R. E. Summons, S. W. Chisholm, Bacterial Vesicles in Marine Ecosystems. *Science (80-.).* **343**, 183–186 (2014).

4. S. J. Biller, P. M. Berube, D. Lindell, S. W. Chisholm, Prochlorococcus: the structure and function of collective diversity. *Nat. Rev. Microbiol.* **13**, 13–27 (2015).

5. P. Flombaum, J. L. Gallegos, R. A. Gordillo, J. Rincón, L. L. Zabala, N. Jiao, D. M. Karl, W. K. W. Li, M. W. Lomas, D. Veneziano, C. S. Vera, J. A. Vrugt, A. C. Martiny, Present and future global distributions of the marine Cyanobacteria Prochlorococcus and Synechococcus. *Proc. Natl. Acad. Sci.* **110**, 9824–9829 (2013).

6. S. Bertilsson, O. Berglund, M. J. Pullin, S. W. Chisholm, Release of dissolved organic matter by Prochlorococcus. *Vie Milieu/Life Environ.*, 225–231 (2005).

7. D. Roth-Rosenberg, D. Aharonovich, A. W. Omta, M. J. Follows, D. Sher, Dynamic macromolecular composition and high exudation rates in Prochlorococcus. *Limnol. Oceanogr.* **66**,

1759–1773 (2021).

8. D. C. O. Thornton, Dissolved organic matter (DOM) release by phytoplankton in the contemporary and future ocean. *Eur. J. Phycol.* **49**, 20–46 (2014).

9. A. R. Matteson, J. M. Rowe, A. J. Ponsero, T. M. Pimentel, P. W. Boyd, S. W. Wilhelm, High abundances of cyanomyoviruses in marine ecosystems demonstrate ecological relevance. *FEMS Microbiol. Ecol.* **84**, 223–234 (2013).

10. M. C. G. Carlson, F. Ribalet, I. Maidanik, B. P. Durham, Y. Hulata, S. Ferrón, J. Weissenbach, N. Shamir, S. Goldin, N. Baran, B. B. Cael, D. M. Karl, A. E. White, E. V. Armbrust, D. Lindell, Viruses affect picocyanobacterial abundance and biogeography in the North Pacific Ocean. *Nat. Microbiol.* **7**, 570–580 (2022).

11. N. Mruwat, M. C. G. Carlson, S. Goldin, F. Ribalet, S. Kirzner, Y. Hulata, S. J. Beckett, D. Shitrit, J. S. Weitz, E. V. Armbrust, D. Lindell, A single-cell polony method reveals low levels of infected Prochlorococcus in oligotrophic waters despite high cyanophage abundances. *ISME J.* **15**, 41–54 (2021).

12. S. J. Beckett, D. Demory, A. R. Coenen, J. R. Casey, M. Dugenne, C. L. Follett, P. Connell, M. C. G. Carlson, S. K. Hu, S. T. Wilson, D. Muratore, R. A. Rodriguez-Gonzalez, S. Peng, K. W. Becker, D. R. Mende, E. V. Armbrust, D. A. Caron, D. Lindell, A. E. White, F. Ribalet, J. S. Weitz, Disentangling top-down drivers of mortality underlying diel population dynamics of Prochlorococcus in the North Pacific Subtropical Gyre. *Nat. Commun.* **15**, 2105 (2024).

13. F. Ribalet, J. Swalwell, S. Clayton, V. Jiménez, S. Sudek, Y. Lin, Z. I. Johnson, A. Z. Worden, E. V. Armbrust, Light-driven synchrony of Prochlorococcus growth and mortality in the subtropical Pacific gyre. *Proc. Natl. Acad. Sci.* **112**, 7–11 (2015).

14. D. Roth-rosenberg, D. Aharonovich, A. Omta, M. J. Follows, D. Sher, Dynamic macromolecular

composition and high exudation rates in Prochlorococcus. *bioRxiv* (2020).

15. J. R. Casey, R. M. Boiteau, M. K. M. Engqvist, Z. V Finkel, G. Li, J. Liefer, C. L. Müller, N. Muñoz, M. J. Follows, Basin-scale biogeography of marine phytoplankton reflects cellular-scale optimization of metabolism and physiology. *Sci. Adv.* **8**, eabl4930 (2022).

16. R. J. Geider, J. La Roche, Redfield revisited: Variability of C:N:P in marine microalgae and its biochemical basis. *Eur. J. Phycol.* **37**, 1–17 (2002).

17. J. D. Liefer, A. Garg, M. H. Fyfe, A. J. Irwin, I. Benner, C. M. Brown, M. J. Follows, A. W. Omta, Z. V. Finkel, The macromolecular basis of phytoplankton C:N:P under nitrogen starvation. *Front. Microbiol.* **10**, 1–16 (2019).

18. L. F. Jover, T. C. Effler, A. Buchan, S. W. Wilhelm, J. S. Weitz, The elemental composition of virus particles: Implications for marine biogeochemical cycles. *Nat. Rev. Microbiol.* **12**, 519–528 (2014).

19. L. R. Thompson, Q. Zeng, L. Kelly, K. H. Huang, A. U. Singer, J. Stubbe, S. W. Chisholm, Phage auxiliary metabolic genes and the redirection of cyanobacterial host carbon metabolism. *Proc. Natl. Acad. Sci. U. S. A.* **108**, E757-64 (2011).

20. N. Y. D. Ankrah, A. L. May, J. L. Middleton, D. R. Jones, M. K. Hadden, J. R. Gooding, G. R. Lecleir, S. W. Wilhelm, S. R. Campagna, A. Buchan, Phage infection of an environmentally relevant marine bacterium alters host metabolism and lysate composition. *ISME J.* **8**, 1089–1100 (2014).

21. A. Chevallereau, B. G. Blasdel, J. De Smet, M. Monot, M. Zimmermann, M. Kogadeeva, U. Sauer, P. Jorth, M. Whiteley, L. Debarbieux, R. Lavigne, Next-Generation "-omics" Approaches Reveal a Massive Alteration of Host RNA Metabolism during Bacteriophage Infection of Pseudomonas aeruginosa. *PLoS Genet.* **12**, 1–20 (2016).

22. X. Xiao, W. Guo, X. Li, C. Wang, X. Chen, X. Lin, M. G. Weinbauer, Q. Zeng, N. Jiao, R. Zhang, Viral Lysis Alters the Optical Properties and Biological Availability of Dissolved Organic Matter Derived from Prochlorococcus Picocyanobacteria. *Appl. Environ. Microbiol.* **87**, 1–19 (2021).

23. X. Fang, Y. Liu, Y. Zhao, Y. Chen, R. Liu, Q. L. Qin, G. Li, Y. Z. Zhang, W. Chan, W. R. Hess, Q. Zeng, Transcriptomic responses of the marine cyanobacterium Prochlorococcus to viral lysis products. *Environ. Microbiol.* **21**, 2015–2028 (2019).

24. F. Azam, F. Malfatti, Microbial structuring of marine ecosystems. *Nat. Rev. Microbiol.* **5**, 782–791 (2007).

25. S. J. Biller, A. Coe, S. E. Roggensack, S. W. Chisholm, Heterotroph Interactions Alter Prochlorococcus Transcriptome Dynamics during Extended Periods of Darkness. *mSystems* **3**, 1–18 (2018).

26. R. Braakman, M. J. Follows, S. W. Chisholm, Metabolic evolution and the self-organization of ecosystems. *Proc. Natl. Acad. Sci.* **114**, E3091–E3100 (2017).

27. B. C. Calfee, L. D. Glasgo, E. R. Zinser, Prochlorococcus Exudate Stimulates Heterotrophic Bacterial Competition with Rival Phytoplankton for Available Nitrogen. *MBio* **13** (2022).

28. J. W. Becker, S. L. Hogle, K. Rosendo, S. W. Chisholm, Co-culture and biogeography of Prochlorococcus and SAR11. *ISME J.* **13**, 1506–1519 (2019).

29. E. B. Kujawinski, R. Braakman, K. Longnecker, J. W. Becker, S. W. Chisholm, K. Dooley, M. C. Kido Soule, G. J. Swarr, K. Halloran, Metabolite diversity among representatives of divergent Prochlorococcus ecotypes. *mSystems* **8** (2023).

30. S. Givati, E. Forchielli, D. Aharonovich, N. Barak, O. Weissberg, N. Belkin, E. Rahav, D. Segrè, D. Sher, Diversity in the utilization of different molecular classes of dissolved organic matter by heterotrophic marine bacteria. *Appl. Environ. Microbiol.* **90**, e00256-24 (2024).

31. M. N. Haider, M. M. Iqbal, M. Nishimura, E. Ikemoto, M. Ijichi, K. Kogure, Bacterial response to glucose addition: growth and community structure in seawater microcosms from North Pacific Ocean. *Sci. Rep.* **13**, 341 (2023).

32. H. Eilers, J. Pernthaler, R. Amann, Succession of Pelagic Marine Bacteria during Enrichment: a Close Look at Cultivation-Induced Shifts. *Appl. Environ. Microbiol.* **66**, 4634–4640 (2000).

33. F. Baltar, D. Lundin, J. Palovaara, I. Lekunberri, T. Reinthaler, G. J. Herndl, J. Pinhassi, Prokaryotic Responses to Ammonium and Organic Carbon Reveal Alternative CO2 Fixation Pathways and Importance of Alkaline Phosphatase in the Mesopelagic North Atlantic. *Front. Microbiol.* **7**, 1–19 (2016).

34. J. S. Weitz, C. A. Stock, S. W. Wilhelm, L. Bourouiba, M. L. Coleman, A. Buchan, M. J. Follows, J. A. Fuhrman, L. F. Jover, J. T. Lennon, M. Middelboe, D. L. Sonderegger, C. A. Suttle, B. P. Taylor, T. Frede Thingstad, W. H. Wilson, K. Eric Wommack, A multitrophic model to quantify the effects of marine viruses on microbial food webs and ecosystem processes. *ISME J.* **9**, 1352–1364 (2015).

35. X. Ma, M. L. Coleman, J. R. Waldbauer, Distinct molecular signatures in dissolved organic matter produced by viral lysis of marine cyanobacteria. *Environ. Microbiol.* **20**, 3001–3011 (2018).

36. M. G. Weinbauer, O. Bonilla-findji, A. M. Y. M. Chan, J. R. Dolan, S. M. Short, Synechococcus growth in the ocean may depend on the lysis of heterotrophic bacteria. *J. Plankton Res.* **33**, 1465–1476 (2011).

37. J. Pourtois, C. E. Tarnita, J. A. Bonachela, Impact of Lytic Phages on Phosphorus- vs. Nitrogen-Limited Marine Microbes. *Front. Microbiol.* **11** (2020).

38. M. G. Weinbauer, Ecology of prokaryotic viruses. *FEMS Microbiol. Rev.* **28**, 127–181 (2004).

39. E. J. Shelford, M. Middelboe, E. F. Møller, C. A. Suttle, Virus-driven nitrogen cycling enhances

phytoplankton growth. *Aquat. Microb. Ecol.* **66**, 41–46 (2012).

40. R. . Sterner, J. . Elser, *Ecological Stoichiometry: The Biology of Elements from Molecules to the Biosphere* (2002).

41. A. R. Moreno, A. C. Martiny, Ecological Stoichiometry of Ocean Plankton. *Ann. Rev. Mar. Sci.* **10**, 43–69 (2018).

42. D. Sher, D. Segrè, M. J. Follows, Quantitative principles of microbial metabolism shared across scales. *Nat. Microbiol.* **9**, 1940–1953 (2024).

43. M. Grossowicz, D. Roth-rosenberg, D. Aharonovich, J. Silverman, M. J. Follows, D. Sher, Prochlorococcus in the lab and in silico : The importance of representing exudation. doi: 10.1002/lno.10463 (2017).

44. T. Ni, Q. Zeng, Diel Infection of Cyanobacteria by Cyanophages. *Front. Mar. Sci.* **2**, 1–7 (2016).

45. S. J. Blazewicz, R. L. Barnard, R. A. Daly, M. K. Firestone, Evaluating rRNA as an indicator of microbial activity in environmental communities: Limitations and uses. *ISME J.* **7**, 2061–2068 (2013).

46. M. Breitbart, L. R. Thompson, C. A. Suttle, M. B. Sullivan, Exploring the vast diversity of marine viruses. *Oceanography* **20**, 135–139 (2007).

47. L. R. Thompson, Q. Zeng, S. W. Chisholm, Gene Expression Patterns during Light and Dark Infection of Prochlorococcus by Cyanophage. *PLoS One* **11**, e0165375 (2016).

48. C. M. Mizuno, C. Guyomar, S. Roux, R. Lavigne, F. Rodriguez-Valera, M. B. Sullivan, R. Gillet, P. Forterre, M. Krupovic, Numerous cultivated and uncultivated viruses encode ribosomal proteins. *Nat. Commun.* **10**, 752 (2019).

49. L.-X. Chen, A. L. Jaffe, A. L. Borges, P. I. Penev, T. C. Nelson, L. A. Warren, J. F. Banfield,

Phage-encoded ribosomal protein S21 expression is linked to late-stage phage replication. *ISME Commun.* **2**, 1–10 (2022).

50. J. D. Brüwer, C. Sidhu, Y. Zhao, A. Eich, L. Rößler, L. H. Orellana, B. M. Fuchs, Globally occurring pelagiphage infections create ribosome-deprived cells. *Nat. Commun.* **15**, 3715 (2024).

51. R. Laurenceau, N. Raho, M. Forget, A. A. Arellano, S. W. Chisholm, Frequency of mispackaging of Prochlorococcus DNA by cyanophage. *ISME J.* **15**, 129–140 (2021).

52. M. A. Moran, E. B. Kujawinski, A. Stubbins, R. Fatland, L. I. Aluwihare, A. Buchan, B. C. Crump, P. C. Dorrestein, S. T. Dyhrman, N. J. Hess, B. Howe, K. Longnecker, P. M. Medeiros, J. Niggemann, I. Obernosterer, D. J. Repeta, J. R. Waldbauer, Deciphering ocean carbon in a changing world. *Proc. Natl. Acad. Sci. U. S. A.* **113**, 3143–3151 (2016).

53. M. J. Szul, S. P. Dearth, S. R. Campagna, E. R. Zinser, Carbon Fate and Flux in Prochlorococcus under Nitrogen Limitation. *mSystems* **4**, 1–16 (2019).

54. F. Eigemann, E. Rahav, H. Grossart, D. Aharonovich, D. Sher, A. Vogts, M. Voss, Phytoplankton exudates provide full nutrition to a subset of accompanying heterotrophic bacteria via carbon, nitrogen and phosphorus allocation. *Environ. Microbiol.* **24**, 2467–2483 (2022).

55. W. Hu, H. Zhang, X. Lin, R. Liu, M. Bartlam, Y. Wang, Characteristics, Biodiversity, and Cultivation Strategy of Low Nucleic Acid Content Bacteria. *Front. Microbiol.* **13** (2022).

56. P. Lebaron, P. Servais, H. Agogue, C. Courties, F. Joux, Does the High Nucleic Acid Content of Individual Bacterial Cells Allow Us To Discriminate between Active Cells and Inactive Cells in Aquatic Systems ? *Appl. Environ. Microbiol.* **67**, 1775–1782 (2001).

57. A. Alothman, D. López-Sandoval, C. M. Duarte, S. Agustí, Bacterioplankton dark CO 2 fixation in oligotrophic waters. *Biogeosciences* **20**, 3613–3624 (2023).

58. C. Amano, U. Willhelm, T. Reinthaler, R. Hansman, Anaplerotic processes are key contributors to

dark carbon xation in the ocean. (2024).

59. F. Baltar, G. J. Herndl, Ideas and perspectives: Is dark carbon fixation relevant for oceanic primary production estimates? *Biogeosciences* **16**, 3793–3799 (2019).

60. A. Braun, M. Spona-Friedl, M. Avramov, M. Elsner, F. Baltar, T. Reinthaler, G. J. Herndl, C. Griebler, Reviews and syntheses: Heterotrophic fixation of inorganic carbon – significant but invisible flux in environmental carbon cycling. *Biogeosciences* **18**, 3689–3700 (2021).

61. T. Reich, N. Belkin, G. Sisma-Ventura, I. Berman-Frank, E. Rahav, Significant dark inorganic carbon fixation in the euphotic zone of an oligotrophic sea. *Limnol. Oceanogr.* **69**, 1129–1142 (2024).

62. M. Spona-Friedl, A. Braun, C. Huber, W. Eisenreich, C. Griebler, A. Kappler, M. Elsner, Substrate-dependent CO2 fixation in heterotrophic bacteria revealed by stable isotope labelling. *FEMS Microbiol. Ecol.* **96**, 1–13 (2020).

63. F. Eigemann, E. Rahav, H. P. Grossart, D. Aharonovich, M. Voss, D. Sher, Phytoplankton Producer Species and Transformation of Released Compounds over Time Define Bacterial Communities following Phytoplankton Dissolved Organic Matter Pulses. *Appl. Environ. Microbiol.* **89** (2023).

64. S. M. Hügler, M., & Sievert, Beyond the Calvin Cycle: Autotrophic Carbon Fixation in the Ocean. *Ann. Rev. Mar. Sci.* **3**, 261–289 (2011).

65. C. F. Kranzler, D. A. Busono, G. J. Walsh, A. C. Carrillo, K. D. Bidle, K. Thamatrakoln, Taxonomically distinct diatom viruses differentially impact microbial processing of organic matter. *Sci. Adv.* **11** (2025).

66. S. Ofaim, S. Sulheim, E. Almaas, D. Sher, D. Segrè, Dynamic Allocation of Carbon Storage and Nutrient-Dependent Exudation in a Revised Genome-Scale Model of Prochlorococcus. *Front.*

Genet. **12**, 1–21 (2021).

67. D. Forchielli, E., Sher, D., & Segrè, Metabolic phenotyping of marine heterotrophs on refactored media reveals diverse metabolic adaptations and lifestyle strategies. *Msystems* **7**, e00070-22 (2022).

68. M. Landa, A. S. Burns, S. J. Roth, M. A. Moran, Bacterial transcriptome remodeling during sequential co-culture with a marine dinoflagellate and diatom. *ISME J.* **11**, 2677–2690 (2017).

69. J. Á. Moreno-Cabezuelo, G. Gómez-Baena, J. Díez, J. M. García-Fernández, Integrated Proteomic and Metabolomic Analyses Show Differential Effects of Glucose Availability in Marine Synechococcus and Prochlorococcus. *Microbiol. Spectr.* **11** (2023).

70. W. D. Swingley, S. Sadekar, S. D. Mastrian, H. J. Matthies, J. Hao, H. Ramos, C. R. Acharya, A. L. Conrad, H. L. Taylor, L. C. Dejesa, M. K. Shah, M. E. O'Huallachain, M. T. Lince, R. E. Blankenship, J. T. Beatty, J. W. Touchman, The Complete Genome Sequence of Roseobacter denitrificans Reveals a Mixotrophic Rather than Photosynthetic Metabolism. *J. Bacteriol.* **189**, 683–690 (2007).

71. F. X. Ferrer-González, B. Widner, N. R. Holderman, J. Glushka, A. S. Edison, E. B. Kujawinski, M. A. Moran, Resource partitioning of phytoplankton metabolites that support bacterial heterotrophy. *ISME J.* **15**, 762–773 (2021).

72. B. Kieft, Z. Li, S. Bryson, R. L. Hettich, C. Pan, X. Mayali, R. S. Mueller, Phytoplankton exudates and lysates support distinct microbial consortia with specialized metabolic and ecophysiological traits. *Proc. Natl. Acad. Sci.* **118**, 1–12 (2021).

73. M. A. Moran, R. Belas, M. A. Schell, J. M. González, F. Sun, S. Sun, B. J. Binder, J. Edmonds, W. Ye, B. Orcutt, E. C. Howard, C. Meile, W. Palefsky, A. Goesmann, Q. Ren, I. Paulsen, L. E. Ulrich, L. S. Thompson, E. Saunders, A. Buchan, Ecological Genomics of Marine Roseobacters.

Appl. Environ. Microbiol. **73**, 4559–4569 (2007).

74. A. Hameed, K. V. Suchithra, S.-Y. Lin, P. Stothard, C.-C. Young, Genomic potential for inorganic carbon sequestration and xenobiotic degradation in marine bacterium Youngimonas vesicularis CC-AMW-ET affiliated to family Paracoccaceae. *Antonie Van Leeuwenhoek* **116**, 1247–1259 (2023).

75. R. Noble, J. Fuhrman, Breakdown and microbial uptake of marine viruses and other lysis products. *Aquat. Microb. Ecol.* **20**, 1–11 (1999).

76. K. M. J. Mayers, C. Kuhlisch, J. T. R. Basso, M. R. Saltvedt, A. Buchan, R.-A. Sandaa, Grazing on Marine Viruses and Its Biogeochemical Implications. *MBio* **14** (2023).

77. M. Middelboe, N. O. G. Jørgensen, Viral lysis of bacteria: an important source of dissolved amino acids and cell wall compounds. *J. Mar. Biol. Assoc. United Kingdom* **86**, 605–612 (2006).

78. Z. Dubinsky, I. Berman-Frank, Uncoupling primary production from population growth in photosynthesizing organisms in aquatic ecosystems. *Aquat. Sci.* **63**, 4–17 (2001).

79. Z. Wu, S. Dutkiewicz, O. Jahn, D. Sher, A. White, M. J. Follows, Modeling Photosynthesis and Exudation in Subtropical Oceans. *Global Biogeochem. Cycles* **35** (2021).

80. L. R. Moore, A. Coe, E. R. Zinser, M. A. Saito, M. B. Sullivan, D. Lindell, K. Frois-Moniz, J. Waterbury, S. W. Chisholm, Culturing the marine cyanobacterium Prochlorococcus. *Limnol. Oceanogr. Methods* **5**, 353–362 (2007).

81. M. B. Sullivan, K. H. Huang, J. C. Ignacio-Espinoza, A. M. Berlin, L. Kelly, P. R. Weigele, A. S. DeFrancesco, S. E. Kern, L. R. Thompson, S. Young, C. Yandava, R. Fu, B. Krastins, M. Chase, D. Sarracino, M. S. Osburne, M. R. Henn, S. W. Chisholm, Genomic analysis of oceanic cyanobacterial myoviruses compared with T4-like myoviruses from diverse hosts and environments. *Environ. Microbiol.* **12**, 3035–3056 (2010).

82. J. J. Morris, R. Kirkegaard, M. J. Szul, Z. I. Johnson, E. R. Zinser, Facilitation of robust growth of Prochlorococcus colonies and dilute liquid cultures by “helper” heterotrophic bacteria. *Appl. Environ. Microbiol.* **74**, 4530–4534 (2008).

83. P. K. Smith, R. I. Krohn, G. T. Hermanson, A. K. Mallia, F. H. Gartner, M. D. Provenzano, E. K. Fujimoto, N. M. Goeke, B. J. Olson, D. C. Klenk, Measurement of protein using bicinchoninic acid. *Anal. Biochem.* **150**, 76–85 (1985).

84. P. Chomczynski, N. Sacchi, Single-step method of RNA isolation by acid guanidinium thiocyanate-phenol-chloroform extraction. *Anal. Biochem.* **1**, 581–585 (1987).

85. J. Marmur, A procedure for the isolation of deoxyribonucleic acid from micro-organisms. *J. Mol. Biol.* **3**, 208-IN1 (1961).

86. M. Simon, F. Azam, Protein content and protein synthesis rates of planktonic marine bacteria. *Mar. Ecol. Prog. Ser.* **51**, 201–213 (1989).

87. T. Reich, T. Ben-Ezra, N. Belkin, A. Tsemel, D. Aharonovich, D. Roth-Rosenberg, S. Givati, M. Bialik, B. Herut, I. Berman-Frank, M. Frada, M. D. Krom, Y. Lehahn, E. Rahav, D. Sher, A year in the life of the Eastern Mediterranean: Monthly dynamics of phytoplankton and bacterioplankton in an ultra-oligotrophic sea. *Deep Sea Res. Part I Oceanogr. Res. Pap.* **182**, 103720 (2022).

88. E. S. Nielsen, The Use of Radio-active Carbon (C14) for Measuring Organic Production in the Sea. *ICES J. Mar. Sci.* **18**, 117–140 (1952).

89. O. Hazan, J. Silverman, G. Sisma-Ventura, T. Ozer, I. Gertman, E. Shoham-Frider, N. Kress, E. Rahav, Mesopelagic Prokaryotes Alter Surface Phytoplankton Production during Simulated Deep Mixing Experiments in Eastern Mediterranean Sea Waters. *Front. Mar. Sci.* **5** (2018).

90. W. Walters, E. R. Hyde, D. Berg-lyons, G. Ackermann, G. Humphrey, A. Parada, J. a Gilbert, J. K. Jansson, Transcribed Spacer Marker Gene Primers for Microbial Community Surveys.

mSystems **1**, e0009-15 (2015).

91. B. J. Callahan, P. J. McMurdie, M. J. Rosen, A. W. Han, A. J. A. Johnson, S. P. Holmes, DADA2: High-resolution sample inference from Illumina amplicon data. *Nat. Methods* **13**, 581–583 (2016).

92. R. F. F. S. C. R Development Core Team, R: A language and environment for statistical computing. (2011).

93. R. Team, RStudio: integrated development for R. RStudio, PBC. (2020).

94. C. Quast, E. Pruesse, P. Yilmaz, J. Gerken, T. Schweer, P. Yarza, J. Peplies, F. O. Glöckner, The SILVA ribosomal RNA gene database project: improved data processing and web-based tools. *Nucleic Acids Res.* **41**, D590–D596 (2012).

95. S. Andrews, FastQC: a quality control tool for high throughput sequence data. (2010).

96. B. Bushnell, J. Rood, E. Singer, BBMerge – Accurate paired shotgun read merging via overlap. *PLoS One* **12**, e0185056 (2017).

97. D. Li, C.-M. Liu, R. Luo, K. Sadakane, T.-W. Lam, MEGAHIT: an ultra-fast single-node solution for large and complex metagenomics assembly via succinct de Bruijn graph. *Bioinformatics* **31**, 1674–1676 (2015).

98. D. Hyatt, G.-L. Chen, P. F. LoCascio, M. L. Land, F. W. Larimer, L. J. Hauser, Prodigal: prokaryotic gene recognition and translation initiation site identification. *BMC Bioinformatics* **11**, 119 (2010).

99. T. Aramaki, R. Blanc-Mathieu, H. Endo, K. Ohkubo, M. Kanehisa, S. Goto, H. Ogata, KofamKOALA: KEGG Ortholog assignment based on profile HMM and adaptive score threshold. *Bioinformatics* **36**, 2251–2252 (2020).

100. F. A. B. von Meijenfeldt, K. Arkhipova, D. D. Cambuy, F. H. Coutinho, B. E. Dutilh, Robust

taxonomic classification of uncharted microbial sequences and bins with CAT and BAT. *Genome Biol.* **20**, 217 (2019).

101. B. Langmead, S. L. Salzberg, Fast gapped-read alignment with Bowtie 2. *Nat. Methods* **9**, 357–359 (2012).

102. D. D. Kang, F. Li, E. Kirton, A. Thomas, R. Egan, H. An, Z. Wang, MetaBAT 2: an adaptive binning algorithm for robust and efficient genome reconstruction from metagenome assemblies. *PeerJ* **7**, e7359 (2019).

103. D. H. Parks, M. Imelfort, C. T. Skennerton, P. Hugenholtz, G. W. Tyson, CheckM: assessing the quality of microbial genomes recovered from isolates, single cells, and metagenomes. *Genome Res.* **25**, 1043–1055 (2015).

104. P.-A. Chaumeil, A. J. Mussig, P. Hugenholtz, D. H. Parks, GTDB-Tk: a toolkit to classify genomes with the Genome Taxonomy Database. *Bioinformatics* **36**, 1925–1927 (2020).

105. E. D. Graham, J. F. Heidelberg, B. J. Tully, Potential for primary productivity in a globally-distributed bacterial phototroph. *ISME J.* **12**, 1861–1866 (2018).

106. G. Korotkevich, V. Sukhov, N. Budin, B. Shpak, M. N. Artyomov, A. Sergushichev, Fast gene set enrichment analysis. (2016). https://doi.org/10.1101/060012.

107. A. M. Eren, Ö. C. Esen, C. Quince, J. H. Vineis, H. G. Morrison, M. L. Sogin, T. O. Delmont, Anvi'o: an advanced analysis and visualization platform for 'omics data. *PeerJ* **3**, e1319 (2015).

108. L. S. with help from S. D.-R. Spencer Graves, Hans-Peter Piepho, multcompView: Visualizations of Paired Comparisons. R package version 0.1-8 (2019). https://cran.r-project.org/package=multcompView.

109. K. M. and D. V. Hadley Wickham, Romain François, Lionel Henry, dplyr: A Grammar of Data Manipulation. R package version 1.1.0 (2023). https://cran.r-project.org/package=dplyr.

110. H. Wickham, H., Averick, M., Bryan, J., Chang, W., McGowan, L., François, R., Grolemund, G., Hayes, A., Henry, L., Hester, J., Kuhn, M., Pedersen, T., Miller, E., Bache, S., Müller, K., Ooms, J., Robinson, D., Seidel, D., Spinu, V., … Yutani, H. Wickham, H., Welcome to the tidyverse. *J. Open Source Softw*. **4**, 1686 (2019).

111. A. Kassambara, rstatix: Pipe-Friendly Framework for Basic Statistical Tests. R package version 0.7.2 (2023). https://rpkgs.datanovia.com/rstatix/.

112. A. Kassambara, ggpubr: "ggplot2" Based Publication Ready Plots. R package version 0.6.0 (2023). https://rpkgs.datanovia.com/ggpubr/.

113. P. Jari Oksanen, Gavin L. Simpson, F. Guillaume Blanchet, Roeland Kindt, M. H. H. S. Legendre, Peter R. Minchin, R.B. O'Hara, Peter Solymos, B. B. Eduard Szoecs, Helene Wagner, Matt Barbour, Michael Bedward, M. D. C. Daniel Borcard, Gustavo Carvalho, Michael Chirico, R. F. Sebastien Durand, Heloisa Beatriz Antoniazi Evangelista, L. Michael Friendly, Brendan Furneaux, Geoffrey Hannigan, Mark O. Hill, T. Lahti, Dan McGlinn, Marie-Helene Ouellette, Eduardo Ribeiro Cunha, C. J. F. T. B. and J. W. Smith, Adrian Stier, vegan: Community Ecology Package. R package version 2.6-2 (2022). https://cran.r-project.org/package=vegan.

114. H. Wickham, ggplot2: Elegant Graphics for Data Analysis. Springer-Verlag New York (2016). https://ggplot2.tidyverse.org.